Studies of granularity of a hadronic calorimeter for tens-of-TeV jets at a 100 TeV *pp* collider

S.V. Chekanov[a], A.V. Kotwal[b,c], J. Proudfoot[a], S. Sen[b], N.V. Tran[c], S.-S. Yu[e], Chih-Hsiang Yeh[e]

[a] *HEP Division, Argonne National Laboratory, 9700 S. Cass Avenue, Argonne, IL 60439, USA.*
[b] *Department of Physics, Duke University, USA*
[c] *Fermi National Accelerator Laboratory*
[d] *Department of Physics, Michigan State University, 220 Trowbridge Road, East Lansing, MI 48824*
[e] *Department of Physics, National Central University, Chung-Li, Taoyuan City 32001, Taiwan*

Abstract

Texts

Keywords: multi-TeV physics, *pp* collider, future hadron colliders, FCC, SppC

1. Introduction

Particle collisions at energies beyond those attained at the LHC will lead to many challenges for detector technologies. Future experiments, such as high-energy LHC (HE-LHC), future circular *pp* colliders of the European initiative, FCC-hh [**?**] and the Chinese initiative, SppC [**?**] will be required to measure high-momentum bosons (W, Z, H) and top quarks with strongly collimated decay products that form jets. Studies of jet substructure can help identify such particles.

The reconstruction of jet substructure variables for collimated jets with transverse momentum above 10 TeV require an appropriate detector design. The most important for reconstruction of such jets are tracking and calorimeter. Recently, a number of studies [**?** **?** **?**] have been discussed using various fast simulation tools, such as Delphes [**?**], in which momenta of particles are smeared to mimic detector response.

A major step towards the usage of full Geant4 simulation to verify the granularity requirements for calorimeters was made in [**?**]. The studies included in this paper have illustrated a significant impact of granularity of electromagnetic (ECAL) and hadronic (HCAL) calorimeters on the shape of hadronic showers calculated using calorimeter hits for two particles separated by some angle. It was concluded that high granularity is essential in resolving two close-by particles for energies above 100 GeV.

This paper makes another step in understanding understanding of this problem in terms of high-level physics quantities typically used in physics analyses. Similar to the studies presented in [**?**], this paper is based on full Geant4 simulation with realistic jet reconstruction.

Email addresses: chekanov@anl.gov (S.V. Chekanov), ashutosh.kotwal@duke.edu (A.V. Kotwal), proudfoot@anl.gov (J. Proudfoot), sourav.sen@duke.edu (S. Sen), ntran@fnal.gov (N.V. Tran), syu@cern.ch (S.-S. Yu), jwzuzelski18@gmail.com (Chih-Hsiang Yeh)

Preprints: XXX-XXX *January 16, 2018*

2. Simulation of detector response and event reconstruction

The description of the detector and software used for this paper is discussed in [**?**]. We use the SiFCC detector geometry with a software package that represents a versatile environment for simulations of detector performance, testing new technology options, event reconstruction techniques for future 100 TeV colliders. The event samples used in this paper are available from the HepSim database [**?**].

The GEANT4 (version 10.3) [**?**] simulation of calorimeter response was complimented with full reconstruction of calorimeter clusters using the Pandora algorithm [**?** **?**]. Calorimeter clusters were built from calorimeter hits in the ECAL and HCAL after applying the corresponding sampling fractions. No other corrections are applied. Hadronic jets were reconstructed with the FASTJET package [**?**] using the anti-k_T algorithm [**?**] with a distance parameter of 0.5.

3. Studies of effective jet radius

The effective radius is the average of the energy weighted radial distance in $\eta - \phi$ space of jet constituents. Recently, it has been studied for multi-TeV jets in Ref.[**?**].

New we sill study jet splitting the effect of granularity on jet splitting scales. A jet k_T splitting scale [**?**] is defined as a distance measure used to form jets by the k_T recombination algorithm [**?** **?**]. This has been studied by ATLAS [**?**], and more recently in the context of 100 TeV physics [**?**]. The distribution of the splitting scale $\sqrt{d_{12}} = \min(p_T^1, p_T^2) \times \delta R_{12}$ [**?**] at the final stage of the k_T clustering, where two subjets are merged into the final one, is shown in Fig. 2.

4. Studies of signal and background separation using calorimeter clusters

In this section, we study different jet substructure variables and compare their ability to separate the signal and the background for different detector sizes using calorimeter clusters.

Figures 3–5 show the ROC curves of three variables, $c_2^{(1)}$ [**?**] , τ_{21} [**?**], and τ_{32} [**?**], respectively. Three different cell sizes of the HCAL are compared for four collision energies. For different cell sizes with the same signal efficiency, the one with the highest background rejection rate, namely (1-background efficiency), has the highest separate power.

In Figure 3 for the variable $c_2^{(1)}$, the ROC curves of the three detector cell sizes are close to each other for each collision energy. Therefore, this variable is not sensitive to the detector cell size.

For the τ_{21} variable in Figure 4, at 5 TeV, the smallest detector size (1×1 cm) can separate the background from the signal well. However, this is not the usual case as the ROC curves nearly merge together at higher collision energy. In addition, the detector with the bigger size tends to have higher separation power than the smaller detector size in 20 and 40 TeV collision energy.

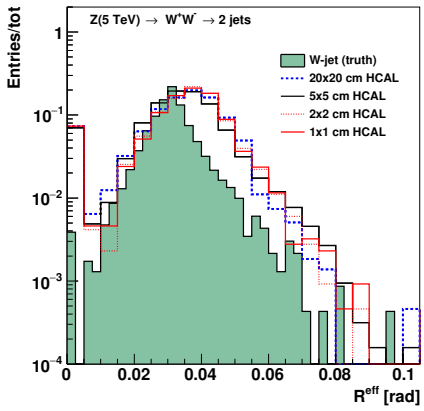

(a) 5 TeV

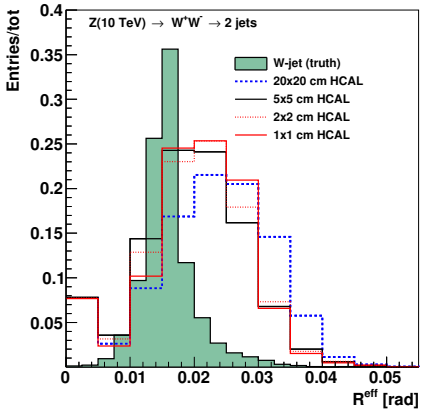

(b) 10 TeV

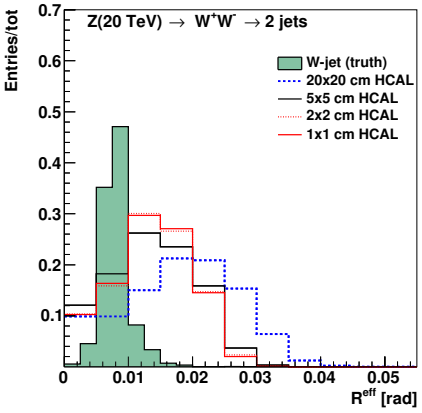

(c) 20 TeV

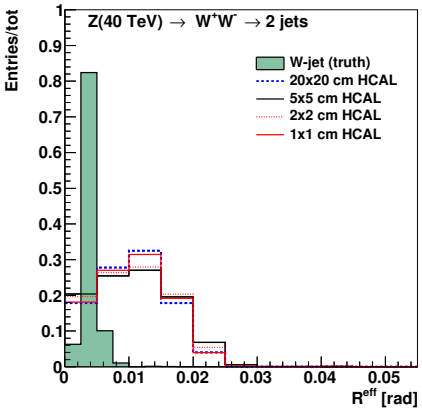

(d) 40 TeV

Figure 1: Jet effective radius for different jet transverse moment and HCAL granularity.

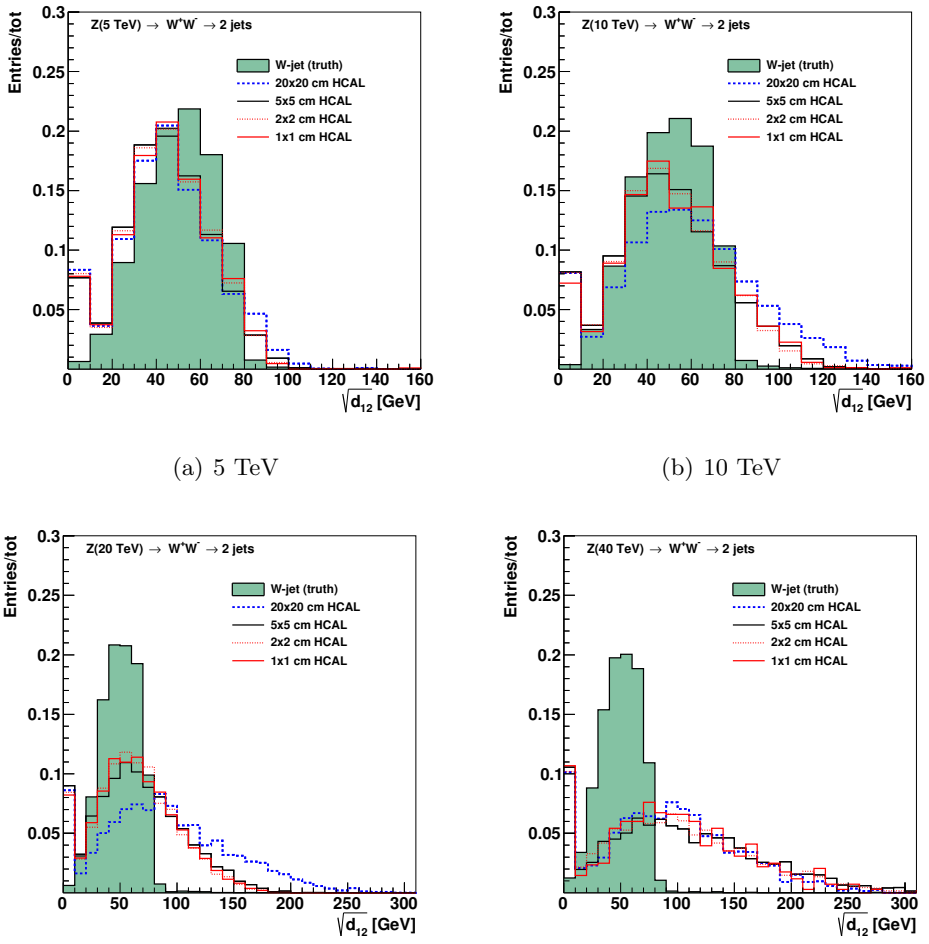

(a) 5 TeV

(b) 10 TeV

(c) 20 TeV

(d) 40 TeV

Figure 2: Jet splitting scale for different jet transverse moment and HCAL granularity.

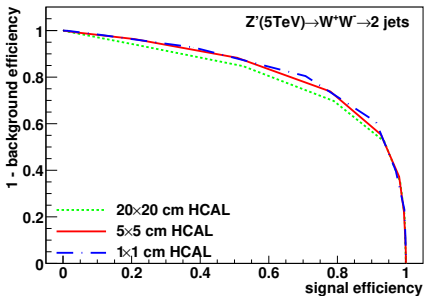

(a) 5 TeV

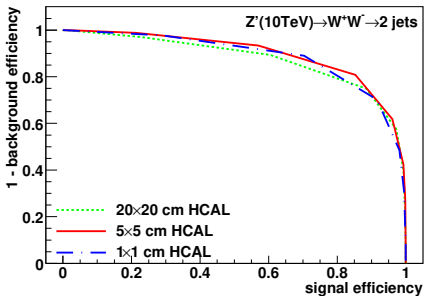

(b) 10 TeV

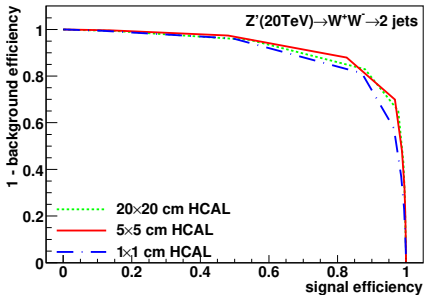

(c) 20 TeV

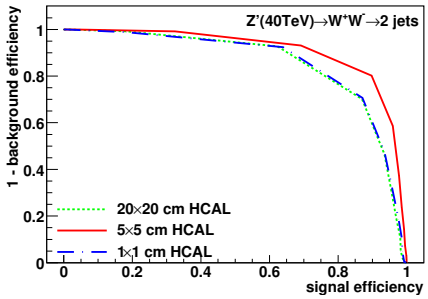

(d) 40 TeV

Figure 3: Signal efficiency versus background rejection rate using $c_2^{(1)}$.The energies of collision at (a)5, (b)10, (c)20, (d)40TeV are shown here. In each picture, the three ROC curves correspond to different detector sizes.

Figure 5 shows the variable τ_{32}, where the smallest detector size has the best separation power for all collision energies.

In conclusion, in all the cases of energy and detector size, the variable $c_2^{(1)}$ has the best separation power compared to the other two variables. In addition, the variable τ_{32} follows the expectation that smaller detector size has better separation power.

5. Studies of signal and background separation using Mann-Whitney U test

In this section, we study different jet substructure variables and compare their ability to separate the signal and the background for different detector sizes using Mann-Whitney U test.

In the Mann Whitney U test by definition, if U value is closed to 0.5, it means two distributions have similar compositions, and we can't distinguish them very well. On the other hand, if U value of two distributions are closed to 0, it means both distributions' compositions are much different from each other. For another point of view, if U value is closed to 0.5, separation power of certain variable is bad, instead, if U value is

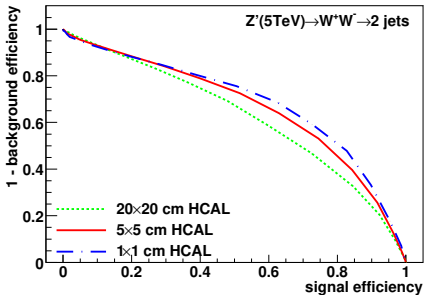

(a) 5 TeV

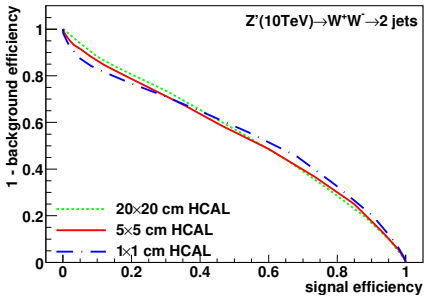

(b) 10 TeV

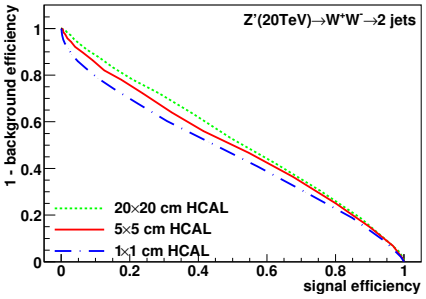

(c) 20 TeV

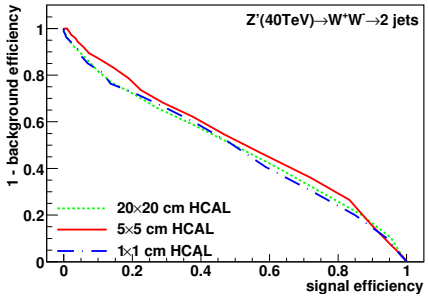

(d) 40 TeV

Figure 4: Signal efficiency versus background rejection rate using τ_{21}.The energies of collision at (a)5, (b)10, (c)20, (d)40TeV are shown here. In each picture, the three ROC curves correspond to different detector sizes.

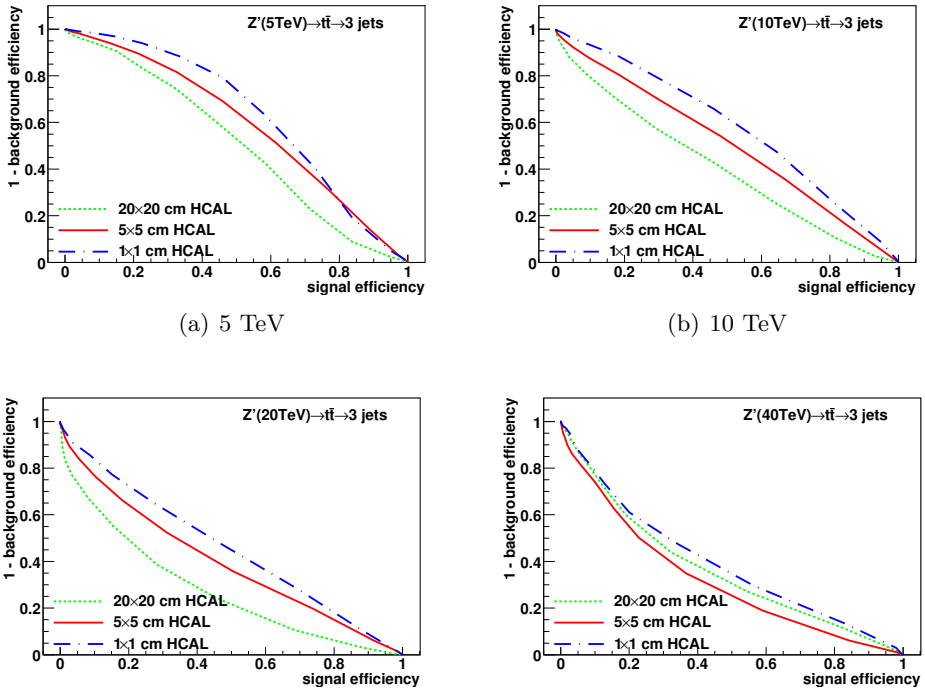

(a) 5 TeV (b) 10 TeV

(c) 20 TeV (d) 40 TeV

Figure 5: Signal efficiency versus background rejection rate using τ_{32}.The energies of collision at (a)5, (b)10, (c)20, (d)40TeV are shown here. In each picture, the three ROC curves correspond to different detector sizes.

closed to 0, separation power is great.

Figure 6 shows the representative samples of the distributions about the U value for τ_{21},τ_{32} in different detector sizes. In τ_{21}, separation power is improved when detector size is smaller, but in τ_{32}, the smallest detector sizes isn't the best one to separate signal and background.

In Figure 7, it shows the summary plots about the clustering in Mann Whitney U test in three different variables. In τ_{21}, 5TeV has better separation power when detector sizes are getting smaller, but when energy higher than that, there is no improvement in smaller detector. In τ_{32}, the case is similar to τ_{21}. Even worse, at some collision energies, bigger detector sizes have better separation power than smaller detector sizes. In $c_2^{(1)}$, all separation power aren't improved by detector sizes. In summary, $c_2^{(1)}$ is the best parameter, because all values are smaller than other parameters compare with the same energy collision, and its separation power don't have the significant improvement in higher energy collision.

In Figure 8 , it shows the summary plots about the rawhit cut at 0.5GeV in Mann Whitney U test in three different variables. In τ_{21}, 5TeV and 10TeV have better separation power in smaller separation power, but when energy higher than that, it won't improve. In τ_{32}, all separation power aren't improved by detector sizes. In $c_2^{(1)}$, we can see in 5,10,20TeV, separation power will be improved slightly, but at 40TeV, it won't improve. In summary, $c_2^{(1)}$ has the highest power separation at highest collision energy.

Acknowledgements

This research was performed using resources provided by the Open Science Grid, which is supported by the National Science Foundation and the U.S. Department of Energy's Office of Science. We gratefully acknowledge the computing resources provided on Blues, a high-performance computing cluster operated by the Laboratory Computing Resource Center at Argonne National Laboratory. Argonne National Laboratory's work was supported by the U.S. Department of Energy, Office of Science under contract DE-AC02-06CH11357. The Fermi National Accelerator Laboratory (Fermilab) is operated by Fermi Research Alliance, LLC under Contract No. DE-AC02-07CH11359 with the United States Department of Energy.

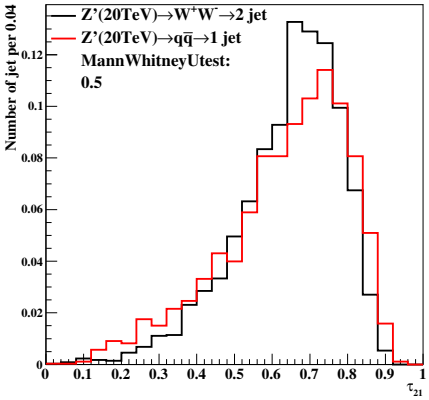

(a) 20×20(cm×cm)

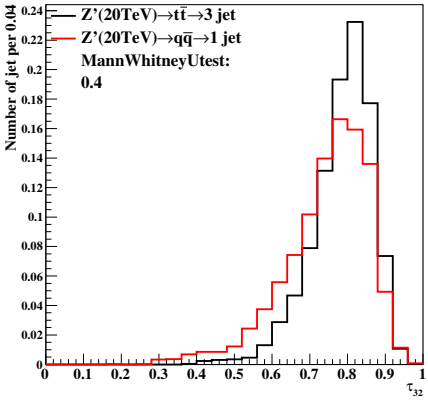

(b) 20×20(cm×cm)

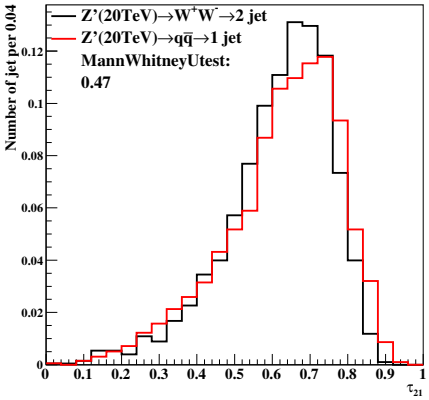

(c) 5×5(cm×cm)

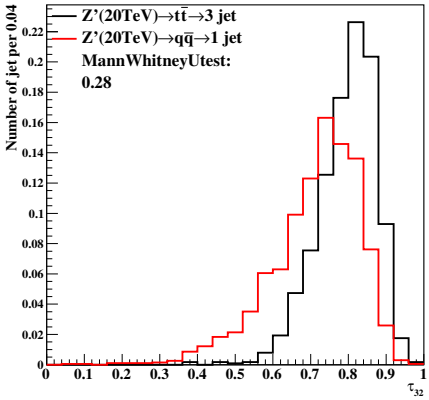

(d) 5×5(cm×cm)

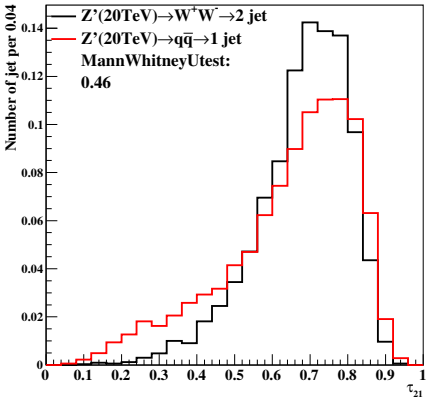

(e) 1×1(cm×cm)

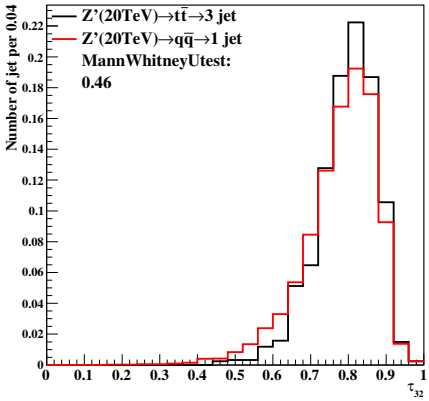

(f) 1×1(cm×cm)

Figure 6: Distributions and U value in 20TeV energy collision for τ_{21},τ_{32} in different detector sizes.

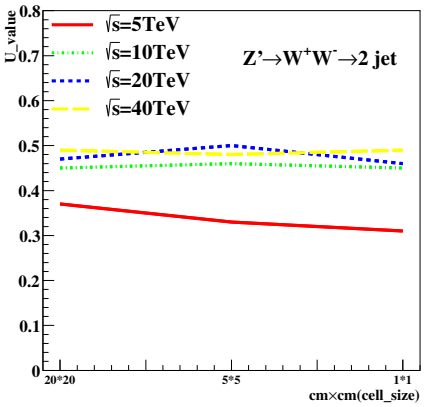

(a) τ_{21}

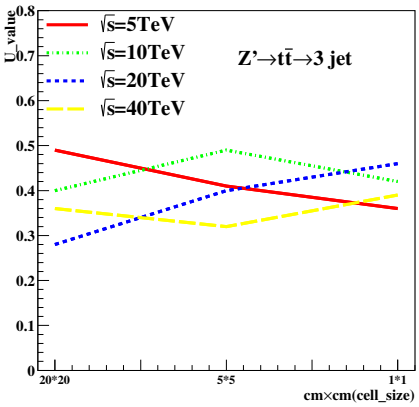

(b) τ_{32}

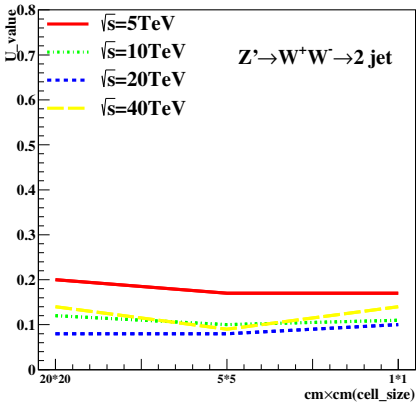

(c) $c_2^{(1)}$

Figure 7: U value of different collision energies correspond to different different detector sizes in cluster. The energies of collision at 5,10, 20, 40TeV are shown in all pictures.

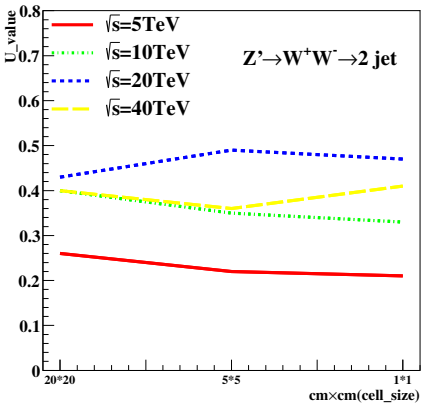

(a) τ_{21}

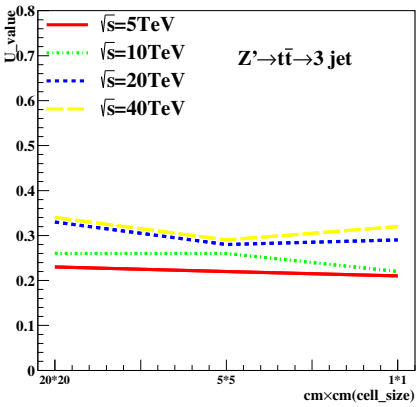

(b) τ_{32}

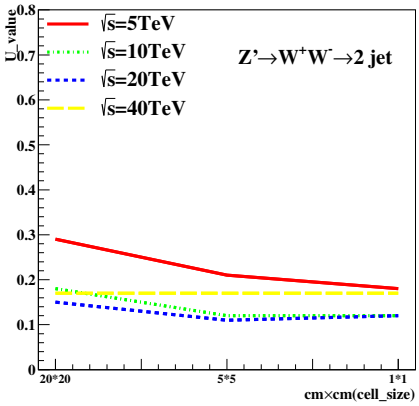

(c) $c_2^{(1)}$

Figure 8: U value of different collision energies correspond to different different detector sizes in rawhit cut at 0.5GeV. The energies of collision at 5,10, 20, 40TeV are shown in all pictures.

References